Diffraction from quasi-one-dimensional crystals

T. Vuković,* I. Milošević, and M. Damnjanović
Faculty of Physics, University of Belgrade, P.O. Box 368, 11001 Belgrade, Serbia
(Received 4 February 2009; published 28 April 2009)

General expressions of diffraction intensity distribution of quasi-one-dimensional crystals are evaluated within kinematical approximation. In order to gain the generality, diffraction intensity has been derived for each of the fifteen conformation classes. Characteristic features of the diffraction patterns are discussed and it is shown how the symmetry can be fully determined from the diffraction intensity distribution. General results are tabulated and their application is illustrated on the (10,10) molybdenum disulfide nanotube.

DOI: 10.1103/PhysRevB.79.165439 PACS number(s): 68.65.−k, 61.05.cc, 61.46.Fg, 24.10.Ht

I. INTRODUCTION

Regular quasi-one-dimensional systems, such as organic and inorganic nanotubes, nanorods, nanowires, stereoregular polymers, etc. have attracted much attention over recent decades. Their most important common characteristic is that all of them are monoperiodic, i.e., they have translational or helical symmetry along a single direction. On the other hand, diffraction is among the most efficient methods for structural characterizations. Due to its well-known relation to system's symmetry,[1,2] it is particularly useful for crystalline samples.

In this paper we give quite general expressions for diffraction intensity distribution of arbitrary quasi-one-dimensional crystals. The method stems from the classification of such structures according to their symmetry. The corresponding line groups are used to decompose quasi-one-dimensional crystals into elementary parts (orbits) preserving the symmetry.[3] After a brief reminder on the structural properties of the line groups (Sec. II), we show (Sec. III) that there are altogether 15 elementary types, i.e., *conformation classes*, of quasi-one-dimensional crystals. Then, within kinematical theory,[4] we calculate analytically the diffraction intensity distributions for each of these classes (Sec. IV), and discuss characteristic features of the diffraction patterns (Sec. V).

II. NECESSARY FACTS ABOUT STRUCTURE OF THE LINE GROUPS

Due to the absence of the crystallographic restriction on the order of the principal axis in monoperiodic systems, there are infinitely many line groups. They are divided into 13 families, $\boldsymbol{L}^{(F)}$ $(F=1,\ldots,13)$, having the form of the (weak-direct) product $\boldsymbol{L}=\boldsymbol{Z}\boldsymbol{P}_n$ of the generalized translation group $\boldsymbol{Z}$ and point factor $\boldsymbol{P}_n$. Generalized translations form infinite cyclic group of screw axis (helical group) $\boldsymbol{T}_Q(f)$ or glide plane $\boldsymbol{T}'(a/2)$, generated by $(C_Q|f)$ and $(\sigma_v|a/2)$. The point factor $\boldsymbol{P}_n$ (n is the order of the principle axis) belongs to one of the seven classes of axial point groups: $\boldsymbol{C}_n$, $\boldsymbol{S}_{2n}$, $\boldsymbol{C}_{nh}$, $\boldsymbol{D}_n$, $\boldsymbol{C}_{nv}$, $\boldsymbol{D}_{nd}$, and $\boldsymbol{D}_{nh}$. Pure rotations and translations along z axis generate rotohelical subgroup $\boldsymbol{L}^{(1)}=\boldsymbol{T}_Q(f)\boldsymbol{C}_n$ of any line group. It is the whole group for the first family $\boldsymbol{L}^{(1)}$; in the families 2–8 it is halving subgroup, and index-four subgroup in the families 9–13. Corresponding coset representatives, called parities, are given in the third column of Table II.

For rational values of $Q=q/r$, there is a pure translational subgroup of $\boldsymbol{L}^{(1)}$ (and $\boldsymbol{L}$), and such groups we call *commensurate* to distinguish from the *incommensurate* ones. For a commensurate first family group, it is possible to choose integers q and r such that $q=\tilde{q}n$, and a number $p=\tilde{p}n$ such that $n=\mathrm{GCD}(p,q)$ and $r\tilde{p}=1+s\tilde{q}$ for some integer s; then the translational period and fractional translation are related as $a=\tilde{q}f$, and we write $\boldsymbol{T}_q^r(f)\boldsymbol{C}_n$. The spatial inversion $\mathcal{I}$ maps $\boldsymbol{T}_Q\boldsymbol{C}_n$ into $\boldsymbol{T}_{Q'}\boldsymbol{C}_n=\mathcal{I}\boldsymbol{T}_Q\boldsymbol{C}_n\mathcal{I}$ with $Q'=n$ (i.e., $q'=n$ and $r'=1$) if $Q=n$ (i.e., $q'=n$ and $r=1$) and $Q'=nQ/(Q-n)$ otherwise. These two groups are different unless $Q=q=n,2n$ (i.e., $\tilde{q}=1,2$ and $p=0,n$, respectively, while $r=1$ in both cases) when we get achiral groups: pure translational group $\boldsymbol{T}(a)$ and zigzag group $\boldsymbol{T}_{2n}^1(a/2)$. Only the achiral first family line groups may be combined with parities other than U axis. Thus, the symmetry of an incommensurate and/or *chiral* system is either $\boldsymbol{L}^{(1)}$ or $\boldsymbol{L}^{(5)}=\boldsymbol{T}_Q(f)\boldsymbol{D}_n$. The principle axis order of the isogonal point group is q for commensurate groups, and infinity for incommensurate ones (in the latter case we use convention $q=\infty$).

III. ELEMENTARY QUASI-ONE-DIMENSIONAL CRYSTALS

Each transformation ℓ of the symmetry group $\boldsymbol{L}$ leaves the system invariant, meaning that ℓ maps any particular atom A into another one of the same chemical type, say $A'=\ell A$. The set $S_A=\boldsymbol{L}A$ of atoms obtained by action of all the transformations from $\boldsymbol{L}$ on A is called *orbit* of the atom A. As the orbit is completely determined by the position of any of its atoms, two orbits are ether disjoint or the same. Therefore, orbits make a unique partition of the system by its symmetry group. In fact, they are the simplest system invariant under $\boldsymbol{L}$, i.e., elementary building blocks of any other $\boldsymbol{L}$-invariant system.

Different orbits of the same group are classified with help of the *stabilizer* or *little group* $\boldsymbol{L}_A$ of atom A, being the set of elements ℓ_A of $\boldsymbol{L}$ for which A is a fixed point, i.e., $\ell_A A=A$. Any atom $A_i=y_iA$ from the orbit of A has conjugated (and accordingly isomorphic) stabilizer $\boldsymbol{L}_{A_i}=y_i\boldsymbol{L}_Ay_i^{-1}$. This enables defining of *orbit type* as the set of the orbits with the conjugated stabilizers.[5] Since $\boldsymbol{L}_A$ is a subgroup of $\boldsymbol{L}$, it gives a partition of $\boldsymbol{L}$ into the cosets $y_i\boldsymbol{L}_A$, enabling to get the line-group elements in the form $\ell=y_i\ell_A$. Different coset representatives y_i map A into different atoms, meaning that the set $\boldsymbol{Y}_A$ of the coset representatives, called *transversal*, is bijectively related to the orbit as $S_A=\boldsymbol{Y}_AA$; still, transversal is not unique as y_i can be substituted by any $y_i\ell_A$. Classification of the

orbits of the line groups[3,6] resulted in 74 families of orbit types.

There are different line groups with orbits with identical transversals (but different stabilizers), i.e., with the same configuration. Thorough inspection of the derived orbits of the line groups (taking into account freedom in the choice of the transversal elements) shows that altogether there are 15 families of these different configurations, called *conformation classes*. Thirteen of them are the generic orbit types a_1 of all the line-group families; their transversals are the groups: $\boldsymbol{Y}^{(F)}=\boldsymbol{L}^{(F)}$, with $F=1,\ldots,13$ counting line-group families. The remaining two are linear conformation classes: single and two atom chains along z axis. One of them is generated by the transversals being generalized translations $\boldsymbol{Z}(f)$, which along z axis act as pure translations, $\boldsymbol{Y}^{(14)}=\boldsymbol{T}(f)$. For the other one transversal contains additional z-reversing element p^-, and gets a form $\boldsymbol{Y}=\boldsymbol{Z}+p^-\boldsymbol{Z}$; however, such elements along z axis act as σ_h, implying that these transversals ($\boldsymbol{T}_Q\boldsymbol{D}_1$, $\boldsymbol{T}_Q\boldsymbol{C}_{1h}$, $\boldsymbol{T}_Q\boldsymbol{D}_{1d}$, $\boldsymbol{T}'\boldsymbol{C}_{1h}$, $\boldsymbol{T}+S_{2n}\boldsymbol{T}$, or $\boldsymbol{T}'+S_{2n}\boldsymbol{T}'$, depending on the line-group family) act effectively as $\boldsymbol{Y}^{(15)}=\boldsymbol{T}(f)\boldsymbol{C}_{1h}$. Conveniently, we denote conformation classes by the corresponding transversals.

The symmetry of an orbit of the line group $\boldsymbol{L}$ is usually greater than the line group, as additional (not from $\boldsymbol{L}$) transformations may also leave it invariant (indeed, only combinations of all system's orbits of $\boldsymbol{L}$ called symmetry fixing sets[3] provide the exact symmetry of $\boldsymbol{L}$). This gives *covering symmetry* group $\tilde{\boldsymbol{Y}}$ (full symmetry group of the orbit), which depends only on the transversal $\boldsymbol{Y}$, i.e., of the conformation class. Since the same conformation class may appear as an orbit type of several line groups, it follows that $\tilde{\boldsymbol{Y}}$ is supergroup of all the line groups with an orbit type corresponding to the considered conformation class.

In Table I we list the symmetry of all the different orbits of the line groups. The coordinate frame referred to in the table is such that z axis is vertical while x axis is in vertical mirror or glide plane, if they exist, or coincides with U axis; if none of these symmetry elements exists, then x axis is taken in the horizontal mirror or rotoreflectional plane (leaving its direction arbitrary) while, for the first class, position of x axis is arbitrary. Obviously, symmetry of the linear conformation classes is $\boldsymbol{T}(a)\boldsymbol{D}_{\infty h}$ while symmetry group of a nonlinear orbit is one of the following groups: $\boldsymbol{T}_Q\boldsymbol{D}_n$, $\boldsymbol{T}\boldsymbol{D}_{nd}$, $\boldsymbol{T}'\boldsymbol{S}_{2n}$, $\boldsymbol{T}\boldsymbol{D}_{nh}$, $\boldsymbol{T}'\boldsymbol{C}_{nh}$, $\boldsymbol{T}^1_{2n}\boldsymbol{D}_{nh}$, and $\boldsymbol{T}\boldsymbol{D}_{\infty h}$. Some orbits for special position of orbit representative have even larger symmetry [e.g., orbit type a_1 of the group $\boldsymbol{T}(a)\boldsymbol{S}_{2n}$ for $z=a/4$ has doubled symmetry $\boldsymbol{T}^1_{2n}(a+2)\boldsymbol{D}_{nh}$]. Such special cases of $\boldsymbol{Y}^{(i)}$ are listed immediately bellow row of $\boldsymbol{Y}^{(i)}$; as the conformation class and transversal remain the same, the conditions selecting the special case are given instead. Also, the orbits of the achiral groups ($Q=1,2n$) of the first family have increased symmetry with respect to the chiral ones, and for these special cases of the transversal $\boldsymbol{Y}^{(1)}$, we use notations $\boldsymbol{Y}^{(1_1)}$ and $\boldsymbol{Y}^{(1_2)}$, respectively.

The conformation classes are illustrated in Figs. 1–5, taking from each class one transversal and one position of orbit representative. The elements of symmetry are depicted as follows: the atoms obtained from the orbit representative (red online, while gray in print) by generalized translations and pure rotations are black and purple (also connected by such lines). As for parities, U axis is green while vertical and horizontal mirror planes are orange and gray, respectively, as well as glide and rotoreflectional planes being also with zigzag and circularly shaped; the same color is reserved for the atom obtained by the parity from the representative atom.

IV. DIFFRACTION INTENSITY FOR THE CONFORMATION CLASSES

Scattering intensity $S(\boldsymbol{k})$ of the diffraction on a particular sample depends on the *diffraction vector*, $\boldsymbol{k}=(\boldsymbol{k}_{\rm sc}-\boldsymbol{k}_{\rm in})/2\pi$, proportional to the difference of the scattered and incident wave vectors. Within kinematical diffraction theory, for a system with ith atom positioned at $\boldsymbol{r}_i$, $S(\boldsymbol{k})$ is absolute square of the *scattering amplitude* averaged per atom $F(\boldsymbol{k})$:

$$F(\boldsymbol{k})=\frac{1}{N}\sum_i f_i(\boldsymbol{k})e^{2\pi i\boldsymbol{k}\cdot\boldsymbol{r}_i}. \tag{1}$$

Here $f_i(\boldsymbol{k})$ is the scattering amplitude of the ith atom ($i=1,\ldots,N$); this is positive rapidly decreasing spherically symmetric [i.e., $f_i(\boldsymbol{k})=f_i(k)$] function.

For a system with symmetry group $\boldsymbol{L}$, above expression splits into sums over the orbits. Precisely, we make the set of orbit representatives (symcell), taking an atom A from each orbit. Then the orbit of the atom A consists of $|\boldsymbol{Y}_A|=|\boldsymbol{L}|/|\boldsymbol{S}_A|$ atoms of the same type, where $\boldsymbol{Y}_A$ and $\boldsymbol{S}_A$ are the transversal and stabilizer of A. The total scattering amplitude becomes

$$F(\boldsymbol{k})=\frac{1}{N}\sum_A |\boldsymbol{Y}_A|F_A(\boldsymbol{k}), \tag{2}$$

and can be easily calculated when all amplitudes of the orbits $F_A(\boldsymbol{k})$ are found. The latter are factorized:

$$F_A(\boldsymbol{k})=f_A(\boldsymbol{k})G^{\boldsymbol{Y}_A}(\boldsymbol{k}),\quad G^{\boldsymbol{Y}_A}(\boldsymbol{k})=\sum_{y\in\boldsymbol{Y}_A}\frac{e^{2\pi i\boldsymbol{k}\cdot\boldsymbol{r}_{yA}}}{|\boldsymbol{Y}_A|}. \tag{3}$$

Here $\boldsymbol{r}_{yA}$ is position of the atom yA. The first factor, the atomic scattering amplitude $f_A(\boldsymbol{k})$, bears the physical information on the diffraction power of atom A; in the calculations it is a known input. The second factor $G^{\boldsymbol{Y}_A}(\boldsymbol{k})$ is purely geometrical: it comprises the information on the arrangement of the atoms and depends only on the conformation class. Therefore, it can be calculated *a priori* for each of the fifteen conformation classes. This way the amplitude for arbitrary quasi-one-dimensional system is provided by Eq. (2) [when atomic scattering amplitudes $f_A(\boldsymbol{k})$ are specified] since all orbits of the line groups are exhausted by conformation classes.

Here we perform this task, and calculate geometrical factors for all conformation classes. It is convenient to use cylindrical coordinates. Thus, $\boldsymbol{k}=(k_\perp,\Phi,k_z)$, orbit representative is at $\boldsymbol{r}_A=(D_A/2,\varphi_A,z_A)$, while the other atoms yA are at $\boldsymbol{r}_{yA}=(D_A/2,\varphi_{yA},z_{yA})$. When scalar product $\boldsymbol{k}\cdot\boldsymbol{r}_{yA}=k_\perp\rho_A\cos(\varphi_{yA}-\Phi)+k_zz_{yA}$ is substituted in *Jacobi-Anger expansion* $e^{ix\cos\varphi}=\sum_{l=-\infty}^{+\infty}i^lJ_l(x)e^{il\varphi}$ [here $J_l(x)$ is Bessel function of order l], Eq. (3) becomes

TABLE I. Symmetry of the orbits of the line groups. For each orbit type (column OT) of all line-group families (separated by the horizontal lines), its transversal $\boldsymbol{Y}$, full symmetry group $\widetilde{\boldsymbol{Y}}$, and its isogonal group $\widetilde{\boldsymbol{P}}_I$ are given. Only one appearance of a transversal is labeled (column CC) as the configuration class $\boldsymbol{Y}^{(i)}$ while the other appearances by i only. Special cases are listed below $\boldsymbol{Y}^{(i)}$ row only.

CC	OT	$\boldsymbol{Y}$	$\widetilde{\boldsymbol{Y}}$	$\widetilde{\boldsymbol{P}}_I$	CC	OT	$\boldsymbol{Y}$	$\widetilde{\boldsymbol{Y}}$	$\widetilde{\boldsymbol{P}}_I$
$\boldsymbol{Y}^{(1)}$	a_1	$\boldsymbol{T}_Q(f)\boldsymbol{C}_n$	$\boldsymbol{T}_Q(f)\boldsymbol{D}_n$	$\boldsymbol{D}_q$	$\boldsymbol{Y}^{(9)}$	a_1	$\boldsymbol{T}(f)\boldsymbol{D}_{nd}$	$\boldsymbol{T}(f)\boldsymbol{D}_{nd}$	$\boldsymbol{D}_{nd}$
1_1		$Q=1$	$\boldsymbol{T}(f)\boldsymbol{D}_{nh}$	$\boldsymbol{D}_{nh}$	8		$z=\frac{f}{4}$	$\boldsymbol{T}^1_{2n}(\frac{f}{2})\boldsymbol{D}_{nh}$	$\boldsymbol{D}_{2nh}$
1_2		$Q=2n$	$\boldsymbol{T}^1_{2n}(f)\boldsymbol{D}_{nh}$	$\boldsymbol{D}_{2nh}$	1_2		$z=\frac{f}{4}$	$\boldsymbol{T}^1_{2n}(\frac{f}{2})\boldsymbol{D}_{nh}$	$\boldsymbol{D}_{2nh}$
						a_2			
$\boldsymbol{Y}^{(14)}$	b_1	$\boldsymbol{T}_Q(f)$	$\boldsymbol{T}(f)\boldsymbol{D}_{\infty h}$	$\boldsymbol{D}_{\infty h}$	1_1	c_1	$\boldsymbol{T}(f)\boldsymbol{C}_{nv}$	$\boldsymbol{T}(f)\boldsymbol{D}_{2nh}$	$\boldsymbol{D}_{2nh}$
$\boldsymbol{Y}^{(2)}$	a_1	$\boldsymbol{T}(f)\boldsymbol{S}_{2n}$	$\boldsymbol{T}(f)\boldsymbol{D}_{nd}$	$\mathbf{D}_{nd}$	2	b_1	$\boldsymbol{T}(f)\boldsymbol{D}_n$	$\boldsymbol{T}(f)\boldsymbol{D}_{nd}$	$\boldsymbol{D}_{nd}$
1_1		$z=\frac{f}{2}$	$\boldsymbol{T}(f)\boldsymbol{D}_{2nh}$	$\boldsymbol{D}_{2nh}$	15	d_1	$\boldsymbol{T}(f)\boldsymbol{D}_{1d}$	$\boldsymbol{T}(f)\boldsymbol{D}_{\infty h}$	$\boldsymbol{D}_{\infty h}$
						d_2			
1_2		$z=\frac{f}{4}$	$\boldsymbol{T}^1_{2n}(\frac{f}{2})\boldsymbol{D}_{nh}$	$\boldsymbol{D}_{2nh}$	14	e_1	$\boldsymbol{T}(f)$	$\boldsymbol{T}(f)\boldsymbol{D}_{\infty h}$	$\boldsymbol{D}_{\infty h}$
$\boldsymbol{Y}^{(15)}$	b_1	$\boldsymbol{T}(f)\{e,S_{2n}\}$	$\boldsymbol{T}(f)\boldsymbol{D}_{\infty h}$	$\boldsymbol{D}_{\infty h}$	$\boldsymbol{Y}^{(10)}$	a_1	$\boldsymbol{T}'(f)\boldsymbol{S}_{2n}$	$\boldsymbol{T}'(f)\boldsymbol{S}_{2n}$	$\boldsymbol{D}_{nd}$
							$\varphi=0$		
14		$z=\frac{f}{4}$	$\boldsymbol{T}(\frac{f}{2})\boldsymbol{D}_{\infty h}$	$\boldsymbol{D}_{\infty h}$	1_1		$z=0$	$\boldsymbol{T}(f)\boldsymbol{D}_{2nh}$	$\boldsymbol{D}_{2nh}$
	b_2					a_2			
14	c_1	$\boldsymbol{T}(f)$	$\boldsymbol{T}(f)\boldsymbol{D}_{\infty h}$	$\boldsymbol{D}_{\infty h}$	1_2	a_3	$\boldsymbol{T}'(f)\boldsymbol{C}_n$	$\boldsymbol{T}^1_{2n}(f)\boldsymbol{D}_{nh}$	$\boldsymbol{D}_{2nh}$
$\boldsymbol{Y}^{(3)}$	a_1	$\boldsymbol{T}(f)\boldsymbol{C}_{nh}$	$\boldsymbol{T}(f)\boldsymbol{D}_{nh}$	$\mathbf{D}_{nh}$	15	b_1	$\boldsymbol{T}'(f)\{e,S_{2n}\}$	$\boldsymbol{T}(a)\boldsymbol{D}_{\infty h}$	$\boldsymbol{D}_{\infty h}$
						b_2			
1_1		$z=\frac{f}{4}$	$\boldsymbol{T}(\frac{f}{2})\boldsymbol{D}_{nh}$	$\mathbf{D}_{nh}$	14	c_1	$\boldsymbol{T}'(f)$	$\boldsymbol{T}(a)\boldsymbol{D}_{\infty h}$	$\boldsymbol{D}_{\infty h}$
	a_2								
1_1	b_1	$\boldsymbol{T}(f)\boldsymbol{C}_n$	$\boldsymbol{T}(f)\boldsymbol{D}_{nh}$	$\mathbf{D}_{nh}$	$\boldsymbol{Y}^{(11)}$	a_1	$\boldsymbol{T}(f)\boldsymbol{D}_{nh}$	$\boldsymbol{T}(f)\boldsymbol{D}_{nh}$	$\boldsymbol{D}_{nh}$
15	c_1	$\boldsymbol{T}(f)\boldsymbol{C}_{1h}$	$\boldsymbol{T}(f)\boldsymbol{D}_{\infty h}$	$\boldsymbol{D}_{\infty h}$	6		$z=\frac{f}{4}$	$\boldsymbol{T}(\frac{f}{2})\boldsymbol{D}_{nh}$	$\boldsymbol{D}_{nh}$
	c_2								
14	d_1	$\boldsymbol{T}(f)$	$\boldsymbol{T}(f)\boldsymbol{D}_{\infty h}$	$\boldsymbol{D}_{\infty h}$	3		$\varphi=\frac{\pi}{2n}$	$\boldsymbol{T}(f)\boldsymbol{D}_{2nh}$	$\boldsymbol{D}_{2nh}$
						a_2			
$\boldsymbol{Y}^{(4)}$	a_1	$\boldsymbol{T}^1_{2n}(f)\boldsymbol{C}_{nh}$	$\boldsymbol{T}^1_{2n}(f)\boldsymbol{D}_{nh}$	$\boldsymbol{D}_{2nh}$	6	d_1	$\boldsymbol{T}(f)\boldsymbol{C}_{nv}$	$\boldsymbol{T}(f)\boldsymbol{D}_{nh}$	$\boldsymbol{D}_{nh}$
						b_1			
1_1		$z=\frac{f}{2}$	$\boldsymbol{T}(f)\boldsymbol{D}_{2nh}$	$\boldsymbol{D}_{2nh}$	3	c_1	$\boldsymbol{T}(f)\boldsymbol{C}_{nh}$	$\boldsymbol{T}(f)\boldsymbol{D}_{nh}$	$\boldsymbol{D}_{nh}$
						b_2			
						c_2			
						e_1			
1_2	b_1	$\boldsymbol{T}^1_{2n}(f)\boldsymbol{C}_n$	$\boldsymbol{T}^1_{2n}(f)\boldsymbol{D}_{nh}$	$\boldsymbol{D}_{2nh}$	$\boldsymbol{Y}^{(1_1)}$	f_1	$\boldsymbol{T}(a)\boldsymbol{C}_n$	$\boldsymbol{T}(a)\boldsymbol{D}_{nh}$	$\boldsymbol{D}_{nh}$
15	c_1	$\boldsymbol{T}^1_{2n}(f)\boldsymbol{C}_{1h}$	$\boldsymbol{T}(f)\boldsymbol{D}_{\infty h}$	$\boldsymbol{D}_{\infty h}$	15	g_1	$\boldsymbol{T}(f)\boldsymbol{C}_{1h}$	$\boldsymbol{T}(f)\boldsymbol{D}_{\infty h}$	$\boldsymbol{D}_{\infty h}$
	c_2					g_2			
14	d_1	$\boldsymbol{T}^1_{2n}(f)$	$\boldsymbol{T}(f)\boldsymbol{D}_{\infty h}$	$\boldsymbol{D}_{\infty h}$	14	h_1	$\boldsymbol{T}(f)$	$\boldsymbol{T}(f)\boldsymbol{D}_{\infty h}$	$\boldsymbol{D}_{\infty h}$
$\boldsymbol{Y}^{(5)}$	a_1	$\boldsymbol{T}_Q(f)\boldsymbol{D}_n$	$\boldsymbol{T}_Q(f)\boldsymbol{D}_n$	$\boldsymbol{D}_q$	$\boldsymbol{Y}^{(12)}$	a_1	$\boldsymbol{T}'(f)\boldsymbol{C}_{nh}$	$\boldsymbol{T}'(f)\boldsymbol{C}_{nh}$	$\boldsymbol{D}_{nh}$
2		$Q=1,\varphi=\frac{\pi}{2n}$	$\boldsymbol{T}(f)\boldsymbol{D}_{nd}$	$\boldsymbol{D}_{nd}$	3		$\varphi=0,\frac{\pi}{n}$	$\boldsymbol{T}(f)\boldsymbol{D}_{nh}$	$\boldsymbol{D}_{nh}$
3		$Q=1,\varphi=0$	$\boldsymbol{T}(f)\boldsymbol{D}_{nh}$	$\boldsymbol{D}_{nh}$	4		$\varphi=\frac{\pi}{2n}$	$\boldsymbol{T}^1_{2n}(f)\boldsymbol{D}_{nh}$	$\boldsymbol{D}_{2nh}$
						a_2			
4		$Q=2n,\varphi=0,\frac{\pi}{2n}$	$\boldsymbol{T}^1_{2n}(f)\boldsymbol{D}_{nh}$	$\boldsymbol{D}_{2nh}$	1_1	a_3	$\boldsymbol{T}'(f)\boldsymbol{C}_n$	$\boldsymbol{T}(f)\boldsymbol{C}_{nh}$	$\boldsymbol{C}_{nh}$
	a_2								
	a_3								
	b_1								
1	c_1	$\boldsymbol{T}_Q(f)\boldsymbol{C}_n$	$\boldsymbol{T}_Q(f)\boldsymbol{D}_n$	$\boldsymbol{D}_q$	7	b_1	$\boldsymbol{T}'(f)\boldsymbol{C}_n$	$\boldsymbol{T}(f)\boldsymbol{C}_{nh}$	$\boldsymbol{C}_{nh}$
15	d_1	$\boldsymbol{T}(f)\boldsymbol{D}_1$	$\boldsymbol{T}(f)\boldsymbol{D}_{\infty h}$	$\boldsymbol{D}_{\infty h}$	15	c_1	$\boldsymbol{T}'(f)\boldsymbol{C}_{1h}$	$\boldsymbol{T}(f)\boldsymbol{D}_{\infty h}$	$\boldsymbol{D}_{\infty h}$
	d_2					c_2			
14	e_1	$\boldsymbol{T}(f)$	$\boldsymbol{T}(f)\boldsymbol{D}_{\infty h}$	$\boldsymbol{D}_{\infty h}$	14	d_1	$\boldsymbol{T}'(f)$	$\boldsymbol{T}(f)\boldsymbol{D}_{\infty h}$	$\boldsymbol{D}_{\infty h}$
$\boldsymbol{Y}^{(6)}$	a_1	$\boldsymbol{T}(f)\boldsymbol{C}_{nv}$	$\boldsymbol{T}(f)\boldsymbol{D}_{nh}$	$\boldsymbol{C}_{nv}$	$\boldsymbol{Y}^{(13)}$	a_1	$\boldsymbol{T}^1_{2n}(f)\boldsymbol{D}_{nh}$	$\boldsymbol{T}^1_{2n}(f)\boldsymbol{D}_{nh}$	$\boldsymbol{D}_{2nh}$
1_1		$\varphi=\frac{\pi}{2n}$	$\boldsymbol{T}(f)\boldsymbol{D}_{2nh}$	$\boldsymbol{D}_{2nh}$	4		$\varphi=\frac{\pi}{2n}$	$\boldsymbol{T}(f)\boldsymbol{D}_{2nh}$	$\boldsymbol{D}_{2nh}$
	b_1								
1_1	c_1	$\boldsymbol{T}(f)\boldsymbol{C}_n$	$\boldsymbol{T}(f)\boldsymbol{D}_{nh}$	$\boldsymbol{D}_{nh}$	1_1		$\varphi=\frac{\pi}{2n},z=\frac{f}{4}$	$\boldsymbol{T}(\frac{f}{2})\boldsymbol{D}_{2nh}$	$\boldsymbol{D}_{2nh}$

TABLE I. (*Continued.*)

CC	OT	$\boldsymbol{Y}$	$\tilde{\boldsymbol{Y}}$	$\tilde{\boldsymbol{P}}_I$	CC	OT	$\boldsymbol{Y}$	$\tilde{\boldsymbol{Y}}$	$\tilde{\boldsymbol{P}}_I$
14	d_1	$\boldsymbol{T}(f)$	$\boldsymbol{T}(f)\boldsymbol{D}_{\infty h}$	$\boldsymbol{D}_{\infty h}$	1_1	a_2	$\boldsymbol{T}^1_{2n}(f)\boldsymbol{C}_{nv}$	$\boldsymbol{T}(f)\boldsymbol{D}_{2nh}$	$\boldsymbol{D}_{2nh}$
$\boldsymbol{Y}^{(7)}$	a_1	$\boldsymbol{T}'(f)\boldsymbol{C}_n$	$\boldsymbol{T}'(f)\boldsymbol{C}_{nh}$	$\boldsymbol{D}_{nh}$	4	b_1	$\boldsymbol{T}^1_{2n}(f)\boldsymbol{C}_{nh}$	$\boldsymbol{T}^1_{2n}(f)\boldsymbol{D}_{nh}$	$\boldsymbol{D}_{2nh}$
1_1		$\varphi=0,\frac{\pi}{n}$	$\boldsymbol{T}(f)\boldsymbol{D}_{nh}$	$\boldsymbol{D}_{nh}$	8	d_1	$\boldsymbol{T}^1_{2n}(f)\boldsymbol{C}_{nv}$	$\boldsymbol{T}^1_{2n}(f)\boldsymbol{D}_{nh}$	$\boldsymbol{D}_{2nh}$
						e_1			
1_2		$\varphi=\frac{\pi}{2n}$	$\boldsymbol{T}^1_{2n}(f)\boldsymbol{D}_{nh}$	$\boldsymbol{D}_{2nh}$	$\boldsymbol{Y}^{(1_2)}$	f_1	$\boldsymbol{T}^1_{2n}(f)\boldsymbol{C}_n$	$\boldsymbol{T}^1_{2n}(\frac{a}{2})\boldsymbol{D}_{nh}$	$\boldsymbol{D}_{2nh}$
14	b_1	$\boldsymbol{T}'(f)$	$\boldsymbol{T}(f)\boldsymbol{D}_{\infty h}$	$\boldsymbol{D}_{\infty h}$	15	g_1	$\boldsymbol{T}^1_{2n}(f)\boldsymbol{C}_{1h}$	$\mathbf{T}(f)\mathbf{D}_{\infty h}$	$\boldsymbol{D}_{\infty h}$
						g_2			
$\boldsymbol{Y}^{(8)}$	a_1	$\boldsymbol{T}^1_{2n}(f)\boldsymbol{C}_{nv}$	$\boldsymbol{T}^1_{2n}(f)\boldsymbol{D}_{nh}$	$\boldsymbol{D}_{2nh}$	14	h_1	$\boldsymbol{T}^1_{2n}(f)$	$\mathbf{T}(f)\mathbf{D}_{\infty h}$	$\boldsymbol{D}_{\infty h}$
1_1		$\varphi=\frac{\pi}{2n}$	$\boldsymbol{T}(f)\boldsymbol{D}_{2nh}$	$\boldsymbol{D}_{2nh}$					
1_2	b_1	$\boldsymbol{T}^1_{2n}(f)\boldsymbol{C}_n$	$\boldsymbol{T}^1_{2n}(f)\boldsymbol{D}_{nh}$	$\boldsymbol{D}_{2nh}$					
14	d_1	$\boldsymbol{T}^1_{2n}(f)$	$\boldsymbol{T}(f)\boldsymbol{D}_{\infty h}$	$\boldsymbol{D}_{\infty h}$					

$$G^{Y_A}(\boldsymbol{k}) = \sum_l i^l J_l(d) e^{-il\Phi} \sum_z \frac{e^{il\varphi_{yA}+i2\pi z_{yA}k_z}}{|\boldsymbol{Y}_A|}, \tag{4}$$

where $d=D_A\pi k_\perp$.

It remains to specify this expression for particular conformation classes, i.e., for 15 different transversals $\boldsymbol{Y}^{(i)}$ (Table I). We start with the first conformation class $\boldsymbol{Y}^{(1)}=\boldsymbol{T}_Q(f)\boldsymbol{C}_n$. Substituting general element

$$y = (C_Q|f)^t C_n^s$$

($t=0,\pm1,\pm2,\ldots$, $s=0,\ldots,n-1$) of this transversal in Eq. (4), one gets [$G_A^{(F)}(\boldsymbol{k})$ denotes geometrical factor of class F]

$$G_A^{(1)}(\boldsymbol{k}) = \sum_l i^l J_l(d) e^{-il(\Phi-\varphi_A)} e^{2\pi i k_z z_A} \left(\frac{1}{n}\sum_s e^{il(2\pi/n)s}\right) \times \left(\frac{1}{|T_Q|}\sum_t e^{2\pi i[k_z f+(1/Q)]t}\right). \tag{5}$$

The sum over s vanishes unless $l=\tilde{M}n$ for integer $\tilde{M}$. Then, taking l in this form, we see that the sum over t is nonzero only when the bracket in the exponent is an integer, $\tilde{K}$. This implies that the amplitudes are distributed only within the countable set of planes at

$$k_z = \left(-\frac{n\tilde{M}}{Q}+\tilde{K}\right)/f, \tag{6}$$

named *layer lines*. In particular, the plane $k_z=0$ (obtained for $\tilde{K}=\tilde{M}=0$) is called *equatorial layer line*.

For incommensurate groups each pair of integers $\tilde{K}$ and $\tilde{M}$ uniquely defines one layer line by the constraint

$$\boldsymbol{k}_{\tilde{K}}^{\tilde{M}} = \left(k_\perp, \Phi, \frac{-n\tilde{M}+Q\tilde{K}}{Qf}\right),$$

and geometrical factor along it is a single term with Bessel function $J_{n\tilde{M}}(d)$ (see row $1'$ of Table II). The set of possible values k_z, determined according to Eq. (6) by two integers, is dense in $\mathbb{R}$, i.e., layer lines are quasicontinually distributed.[2]

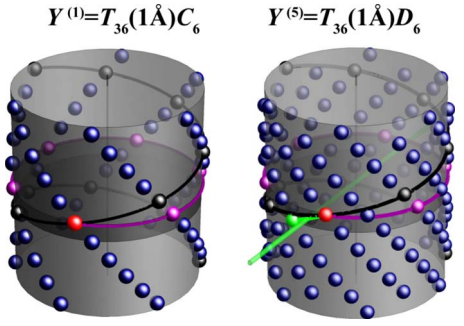

FIG. 1. (Color online) Conformation classes $\boldsymbol{Y}=\boldsymbol{T}_q^r(f)\boldsymbol{P}_n$ illustrated by orbits with $q=36$ Å, $r=5$ Å, $n=6$ Å, $r=6$ Å, and $a=6$ Å and $\boldsymbol{r}_A=(5\text{ Å},5\pi/72,0.45\text{ Å})$.

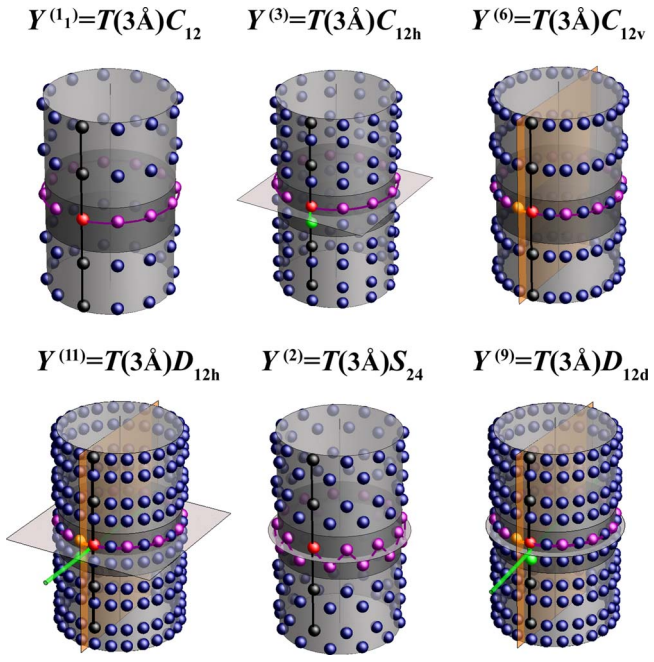

FIG. 2. (Color online) Conformation classes $\boldsymbol{Y}=\boldsymbol{T}(a)\boldsymbol{P}_n$ illustrated by orbits with $n=12$ Å and $a=3$ Å, and $\boldsymbol{r}_A=(4\text{ Å},\pi/25,0.6\text{ Å})$.

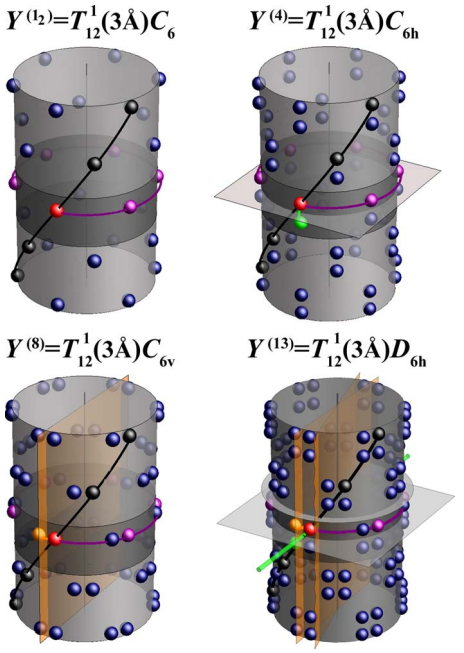

FIG. 3. (Color online) Conformation classes $\boldsymbol{T}^1_{2n}(a/2)\boldsymbol{P}_n$ illustrated by orbits with $n=6$ Å and $a=6$ Å, and $\boldsymbol{r}_A=(4\ \text{Å}, \pi/25, 0.6\ \text{Å})$.

For commensurate groups, layer lines are equidistant, spaced by $1/a$. Indeed, for $k_z=K/a$ (K is an integer), condition (6) becomes Diophantine equation:

$$-r\tilde{M}+\tilde{q}\tilde{K}=K. \tag{7}$$

It is well known that as $\tilde{q}$ and r are coprimes this equation has a set of solutions $\tilde{M}=-K\tilde{p}+M\tilde{q}$ and $\tilde{K}=K\frac{1-r\tilde{p}}{\tilde{q}}-Mr$ ($M=0,\pm1,\ldots$) for each value of K. Thus, summing over M we find the geometrical factor (Table II) of the layer line defined by $\boldsymbol{k}_K=(k_\perp,\Phi,K/a)$. Conveniently, integer K can be used to label the layer lines.

After calculating geometrical factor for the first conformation class, we obtain results for the remaining orbit types (Table II) within two-step procedure. Namely, $\boldsymbol{Y}^{(1)}$ is halving subgroup in the transversals $\boldsymbol{Y}^{(F)}$ for $F=2,\ldots,8$, i.e., $\boldsymbol{Y}^{(F)}=\boldsymbol{Y}^{(1)}+\ell\boldsymbol{Y}^{(1)}$. Therefore, from Eq. (3) it follows that $G_A^{(F)}(\boldsymbol{k}_K)=\frac{1}{2}[G_A^{(1)}(\boldsymbol{k}_K)+G_{\ell A}^{(1)}(\boldsymbol{k}_K)]$, and geometrical factors are easily calculated from that for $\boldsymbol{Y}^{(1)}$. Further, these transversals are halving subgroups of the remaining ones, i.e., $9,\ldots,13$, and the same algorithm applies once again.

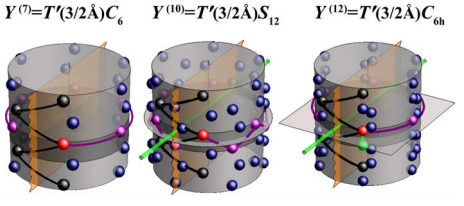

FIG. 4. (Color online) Conformation classes $\boldsymbol{T}'(a/2)\boldsymbol{P}_n$ illustrated by orbits with $n=6$ Å and $a=6$ Å, and $\boldsymbol{r}_A=(4\ \text{Å}, \pi/7, 0.6\ \text{Å})$.

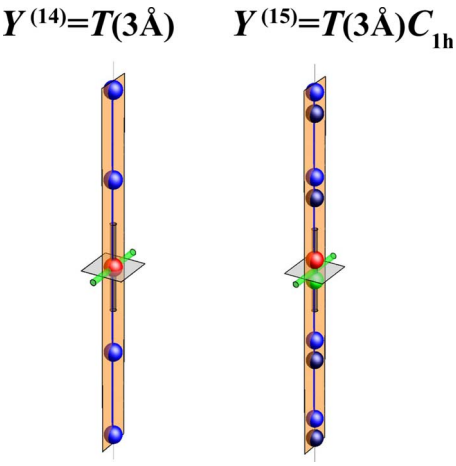

FIG. 5. (Color online) Two linear conformation classes $\boldsymbol{Y}^{(14)}=\boldsymbol{T}(a)$ and $\boldsymbol{Y}^{(15)}=\boldsymbol{T}(a)\boldsymbol{C}_{1h}$ illustrated by orbits with $a=3$ Å and $\boldsymbol{r}_A=(0,0,0.6\ \text{Å})$.

V. ANALYSIS OF DIFFRACTION INTENSITY

The diffraction patterns, representing intensity distribution along particular cross sections of $\boldsymbol{k}$ space, and configuration of the system are neatly related. The symmetry of the scattering intensity distribution $S(\boldsymbol{k})$, being the only observable quantity in diffraction experiments, is direct consequence of the symmetry of the system configuration. Even more, in order to derive, as much as possible, information from diffraction experiments, it is important to understand how particular elements of symmetry are manifested in the diffraction patterns. To this end we note that within a single layer line at k_z, the intensity distribution is a sum of terms being products of a Bessel function, involving radial coordinates $k_\perp$ and D_A, and a trigonometric function of other coordinates (Φ, k_z, φ_A, and z_A). The following analysis shows that the orders of Bessel functions and the specific form of the trigonometric functions are determined by symmetry only: namely, the former are related to the first family subgroup only while the latter depend on the additional parities.

A. Symmetry of intensity distribution

The action of the arbitrary Euclidean transformation $(R|\boldsymbol{f})$ on the scattering intensity is derived from the action on the coordinates:

$$(R|\boldsymbol{f})S(\boldsymbol{k})=\left|\sum_i f_i(k)e^{i2\pi(R^{-1}\boldsymbol{k})\cdot\boldsymbol{r}_i}\right|^2=S(R^{-1}\boldsymbol{k}). \tag{8}$$

Obviously, it is reduced to the action of only orthogonal part on $\boldsymbol{k}$ vectors, meaning that translational part $\boldsymbol{f}$ can be ignored. Elements of the covering symmetry group $\tilde{\boldsymbol{Y}}$ only permute the terms in sum, leaving thus the intensity invariant. When the translational parts of the elements of $\tilde{\boldsymbol{Y}}$ are skipped, isogonal group $\tilde{\boldsymbol{P}}_I$ is obtained. Finally, spatial inversion $\mathcal{I}$ only changes the sign of $\boldsymbol{r}_i$, i.e., it is equivalent to complex conjugation. Thus, $\mathcal{I}$ is a symmetry of the diffraction intensity distribution whether or not it is a symmetry of the system. Summarizing, the symmetry group $\boldsymbol{S}^Y$ of the intensity distri-

TABLE II. Geometrical factors for conformation classes. For each class (column F, primes single out the incommensurate cases), the transversal $\boldsymbol{Y}^{(F)}$, coset representatives with respect to rotohelical subgroup $\boldsymbol{L}^{(1)}$ (column CR), and diffraction space symmetry group $\boldsymbol{S}^{(F)}=\widetilde{\boldsymbol{Y}}_I+\mathcal{I}\widetilde{\boldsymbol{Y}}_I$ (when it depends on the parity of n, the odd case is up) are given. The last column gives geometrical factors $G_A^{(F)}$ in the layer lines specified by $\boldsymbol{k}_K=(k_\perp,\Phi,\frac{K}{a})$ for commensurate and $\boldsymbol{k}_{\widetilde{K}}^{\widetilde{M}}=(k_\perp,\Phi,\frac{Q\widetilde{K}-n\widetilde{M}}{Qf})$ for incommensurate groups; outside them geometrical factors vanish.

F	$\boldsymbol{Y}^{(F)}$	CR	$\boldsymbol{S}^{(F)}$	$G_A^{(F)}(\boldsymbol{k}_K)$ or $G_A^{(F)}(\boldsymbol{k}_{\widetilde{K}}^{\widetilde{M}})$
1	$\boldsymbol{T}_q^r\boldsymbol{C}_n$		$\boldsymbol{D}_{qd}$ $\boldsymbol{D}_{qh}$ $\boldsymbol{D}_{2nh}$	$\Sigma_M i^{Mq-Kp}J_{Mq-Kp}(d)e^{i(Kp-Mq)(\Phi-\varphi_A)}e^{2\pi iK\frac{z_A}{a}}$
1_1	$\boldsymbol{TC}_n$		$\boldsymbol{D}_{nh}$	$\Sigma_M i^{Mn}J_{Mn}(d)e^{-iMn(\Phi-\varphi_A)}e^{2\pi iK\frac{z_A}{a}}$
1_2	$\boldsymbol{T}_{2n}^1\boldsymbol{C}_n$		$\boldsymbol{D}_{2nh}$	$\Sigma_M i^{(2M-K)n}J_{(2M-K)n}(d)e^{i(K-2M)n(\Phi-\varphi_A)}e^{2\pi iK\frac{z_A}{a}}$
$1'$	$\boldsymbol{T}_Q\boldsymbol{C}_n$		$\boldsymbol{D}_{\infty h}$	$i^{n\widetilde{M}}J_{n\widetilde{M}}(d)e^{-in\widetilde{M}(\Phi-\varphi_A)}e^{2\pi i\frac{Q\widetilde{K}-n\widetilde{M}}{Q}\frac{z_A}{f}}$
2	$\boldsymbol{TS}_{2n}$	$\boldsymbol{C}_{2n}\sigma_h$	$\boldsymbol{D}_{nd}$ $\boldsymbol{D}_{2nh}$ $\boldsymbol{D}_{2nh}$	$\Sigma_M i^{M(n+1)}J_{Mn}(d)e^{-iMn(\Phi-\varphi_A)}\cos(2\pi K\frac{z_A}{a}-\frac{M\pi}{2})$
3	$\boldsymbol{TC}_{nh}$	σ_h	$\boldsymbol{D}_{nh}$	$\Sigma_M i^{Mn}J_{Mn}(d)e^{-iMn(\Phi-\varphi_A)}\cos 2\pi K\frac{z_A}{a}$
4	$\boldsymbol{T}_{2n}^1\boldsymbol{C}_{nh}$	σ_h	$\boldsymbol{D}_{2nh}$	$\Sigma_M i^{(2M-K)n}J_{(2M-K)n}(d)e^{i(K-2M)n(\Phi-\varphi_A)}\cos 2\pi K\frac{z_A}{a}$
5	$\boldsymbol{T}_q^r\boldsymbol{D}_n$	U	$\boldsymbol{D}_{qd}$ $\boldsymbol{D}_{qh}$	$\Sigma_M i^{Mq-Kp}J_{Mq-Kp}(d)e^{i(Kp-Mq)\Phi}\cos[(Mq-Kp)\varphi_A+2\pi K\frac{z_A}{a}]$
$5'$	$\boldsymbol{T}_Q\boldsymbol{D}_n$	U	$\boldsymbol{D}_{\infty h}$	$i^{n\widetilde{M}}J_{n\widetilde{M}}(d)e^{-in\widetilde{M}\Phi}\cos(2\pi\frac{Q\widetilde{K}-n\widetilde{M}}{Q}\frac{z_A}{f}-n\widetilde{M}\varphi_A)$
6	$\boldsymbol{TC}_{nv}$	σ_v	$\boldsymbol{D}_{2nh}$ $\boldsymbol{D}_{nh}$ $\boldsymbol{D}_{2nh}$	$\Sigma_M i^{Mn}J_{Mn}(d)e^{-iMn\Phi}e^{i2\pi K\frac{z_A}{a}}\cos Mn\varphi_A$
7	$\boldsymbol{T}'\boldsymbol{C}_n$	$(\sigma_v\vert\frac{a}{2})$	$\boldsymbol{D}_{nh}$	$\Sigma_M i^{Mn+K}J_{Mn}(d)e^{-iMn\Phi}e^{2\pi iK\frac{z_A}{a}}\cos(Mn\varphi_A-\frac{K\pi}{2})$
8	$\boldsymbol{T}_{2n}^1\boldsymbol{C}_{nv}$	σ_v	$\boldsymbol{D}_{2nh}$	$\Sigma_M i^{(2M-K)n}J_{(2M-K)n}(d)e^{i2\pi K\frac{z_A}{a}}e^{i(K-2M)n\Phi}\cos(K-2M)n\varphi_A$
9	$\boldsymbol{TD}_{nd}$	σ_v,U_d,S_{2n}	$\boldsymbol{D}_{nd}$ $\boldsymbol{D}_{2nh}$ $\boldsymbol{D}_{nd}$	$\Sigma_M i^{M(n+1)}J_{Mn}(d)e^{-iMn\Phi}\cos(2\pi K\frac{z_A}{a}-\frac{M\pi}{2})\cos Mn\varphi_A$
10	$\boldsymbol{T}'\boldsymbol{S}_{2n}$	$(\sigma_v\vert\frac{a}{2}),S_{2n},(U_d\vert\frac{a}{2})$	$\boldsymbol{D}_{2nh}$ $\boldsymbol{D}_{2nh}$	$\Sigma_M i^{M(n+1)+K}J_{Mn}(d)e^{-iMn\Phi}\cos(2\pi K\frac{z_A}{a}-\frac{M\pi}{2})\cos(Mn\varphi_A-\frac{K\pi}{2})$
11	$\boldsymbol{TD}_{nh}$	σ_v,U,σ_h	$\boldsymbol{D}_{nh}$ $\boldsymbol{D}_{2nh}$	$\Sigma_M i^{Mn}J_{Mn}(d)e^{-iMn\Phi}\cos 2\pi K\frac{z_A}{a}\cos Mn\varphi_A$
12	$\boldsymbol{T}'\boldsymbol{C}_{nh}$	$(\sigma_v\vert\frac{a}{2}),U,(S_{2n}\vert\frac{a}{2})$	$\boldsymbol{D}_{nh}$	$\Sigma_M i^{Mn+K}J_{Mn}(d)e^{-iMn\Phi}\cos 2\pi K\frac{z_A}{a}\cos(Mn\varphi_A-\frac{K\pi}{2})$
13	$\boldsymbol{T}_{2n}^1\boldsymbol{D}_{nh}$	σ_v,U,σ_h	$\boldsymbol{D}_{2nh}$	$\Sigma_M i^{(2M-K)n}J_{(2M-K)n}(d)e^{i(K-2M)n\Phi}\cos 2\pi K\frac{z_A}{a}\cos(K-2M)n\varphi_A$
14	$\boldsymbol{T}$		$\boldsymbol{D}_{\infty h}$	$e^{i2\pi K\frac{z_A}{a}}$
15	$\boldsymbol{TC}_{1h}$	σ_h	$\boldsymbol{D}_{\infty h}$	$\cos(2\pi K\frac{z_A}{a})$

bution is the extension of the isogonal point group $\widetilde{\boldsymbol{P}}_I$ by the spatial inversion.

This group is determined for each elementary quasi-one-dimensional crystal. Namely, for each conformation class $\boldsymbol{Y}^{(F)}$, we find the isogonal point group $\widetilde{\boldsymbol{P}}_I^{(F)}$ of its symmetry group $\widetilde{\boldsymbol{Y}}^{(F)}$ (Table II). Then, if $\widetilde{\boldsymbol{P}}_I^{(F)}$ contains spatial inversion, the symmetry group $\boldsymbol{S}^{(F)}$ of the intensity distribution is just $\widetilde{\boldsymbol{P}}_I^{(F)}$; otherwise $\mathbf{S}^{(F)}$ is the group $\widetilde{\boldsymbol{P}}_I^{(F)}$ augmented by the spatial inversion, i.e., $\boldsymbol{S}^{(F)}=\widetilde{\boldsymbol{P}}_I^{(F)}+\mathcal{I}\widetilde{\boldsymbol{P}}_I^{(F)}$. As the isogonal point groups of the line groups are well known,[7] it remains to find $\mathbf{S}^{(F)}$ as prescribed (Table II).

To summarize, according to their symmetry, there are three types of scattering intensities. Incommensurate ($\boldsymbol{Y}^{(1')}$, $\boldsymbol{Y}^{(5')}$) and linear conformation classes ($\boldsymbol{Y}^{(14)}$ and $\boldsymbol{Y}^{(15)}$) produce axially symmetric intensities, with symmetry group $\boldsymbol{D}_{\infty h}$; in addition, geometrical factor of the linear systems is constant in each layer line. The remaining classes give distribution with symmetry group of the type $\boldsymbol{D}_{nh}$, except that $\boldsymbol{D}_{nd}$ is obtained for classes $\boldsymbol{Y}^{(1)}$, $\boldsymbol{Y}^{(2)}$, $\boldsymbol{Y}^{(5)}$, $\boldsymbol{Y}^{(6)}$, $\boldsymbol{Y}^{(9)}$, and $\boldsymbol{Y}^{(10)}$ for odd order of the principle axis of the isogonal point group. Obviously, the symmetry of the scattering patterns of the elementary systems is maximally symmetric in a sense that, among seven families of axial point groups, these are the largest ones.

B. Properties related to the first family subgroup

It is evident from Table II that the orders of Bessel functions appearing in the geometrical factor are multiples of n, thus manifesting pure rotational symmetry $\boldsymbol{C}_n$ (for the classes 1 and 5 this follows from the fact that n divides both p and

q). However, which of these multiples are involved in a particular layer line depends on the screw axis. If it is incommensurate, only a single term is included for each of densely distributed layer lines. On the contrary, the intensity of commensurable systems is localized into the equally spaced (by $1/a$) layer lines, and the Kth one contains terms with orders $qM-pK=n(\tilde{q}M-\tilde{p}K)$ ($M=0,\pm 1,\ldots$), differing by multiple of q. Consequently, only if the helical axis is pure translational group $\boldsymbol{T}(a)$ (then $\tilde{q}=1$, $q=n$, and $p=0$), all the multiples nM appear for every layer line. Otherwise, for nontrivial screw axes, various layer lines involve different orders; in fact, as $\tilde{p}$ and $\tilde{q}$ are coprimes, these orders are repeated in every $\tilde{q}$th layer line. This means that, unless additional factors (multiplying Bessel functions) wipe out some terms, radii of the peaks are the same for every $\tilde{q}$th layer line (still, their intensities may differ). This "periodicity" and already established spatial inversion symmetry of the diffraction space (relating layer lines K and $-K$) allow us to consider only the layer lines with $0\leq K\leq \tilde{q}/2$.

Above conclusion about the orders of the Bessel functions may be applied to relate the diffraction patterns to particular screw axes. To this end, denoting by $x_{\alpha,i}$ the position of ith extreme of the Bessel function $J_\alpha(x)$, we note some properties of the Bessel functions important for further analysis. At first, the Bessel functions of the opposite orders have the same extremes, $x_{\alpha,i}=x_{-\alpha,i}$, as it follows from the property $J_{-\alpha}(x)=(-1)^\alpha J_\alpha(x)$. Further, the position of the ith extremum increases with the absolute order $|\alpha|$ of the Bessel function, i.e., if $|\alpha'|>|\alpha|$ then $x_{\alpha',i}>x_{\alpha,i}$. In fact, only for $\alpha=0$, $J_\alpha(x)$ has the extremum at $x_{0,1}=0$; for $\alpha>0$, $J_\alpha(x)$ vanishes at $x=0$, and changes very slowly, remaining almost zero until the region close to the first extremum $x_{\alpha,1}$. Among the orders involved in the geometrical factor of a layer line, the two with the least absolute values (their first extremes are closest to the origin) are denoted by β and β'. Precisely, $\beta\doteq -Kp$ [equal modulo interval $(-q/2,q/2)$] while β' equals $\beta-q$ if $\beta\geq 0$, and $-\beta+q$ otherwise.

Now we note that $\beta=0$ only for $K=0,\pm\tilde{q},\pm 2\tilde{q},\ldots$, i.e., for these layer lines $J_0(d)$ is involved; consequently, only for them do the intensity distributions have broad maximum at $k_\perp=0$. Otherwise, the *intensity gap* appears: the first maximum (bright spot) is at $k_\perp=x_{\beta,1}/\pi D_A>0$. In particular, the narrowest gap is for the layer lines $K=\pm r+s\tilde{q}$ ($=0,\pm 1,\ldots$), since for these values of K the minimal nonzero $\tilde{M}=\mp r\tilde{p}+M\tilde{q}=\mp 1$ appears (for some M), yielding the minimal nonzero order $\alpha=\mp n$ of the allowed Bessel function.

As for the angular dependence of intensity distribution, we note that only a phase factor in each term depends on Φ. As it has unit absolute value, angular modulation of diffraction intensity is due only to the interference between different terms in the absolute square of geometrical factor. The period of the pattern, i.e., the greatest common angular period of all the terms in $S(\boldsymbol{k})$, is $2\pi/q$, manifesting the known invariance of the pattern under the rotations from the isogonal group. Some patterns contain several seemingly solid circles around Z axis, as if the leading terms are axially symmetric. Indeed, $J_{\beta'}(d)$ is negligible for $k_\perp<k_{\beta'}$, where $k_{\beta'}$ is less but close to $x_{\beta',1}/\pi D_A$. Therefore, the only Bessel function relevant in this region around Z axis is $J_\beta(d)$, thus producing almost nonmodulated solid circles at the radii corresponding to its extremes. Their number can be easily found for each layer line while it depends on $k_{\beta'}$, i.e., the criterion of neglecting of $J_{\beta'}(d)$. However, as between two zeros there is always a single extreme of Bessel functions, this number is close to, but not greater than, the number of zeros of $J_\beta(d)$ less than $x_{\beta',1}/\pi D_A$.

Note that the circles do not appear only if $|\beta'|=|\beta|$, i.e., when the two closest to zero orders are opposite. Obviously, this occurs only if $\tilde{q}$ is even and only for the layer lines $K=\pm\tilde{q}/2,\pm 3\tilde{q}/2,\pm 5\tilde{q}/2,\ldots$; since $\tilde{p}$ is odd (as a coprime with $\tilde{q}$) we write $\tilde{p}=2P+1$, and substitute $M-P$ by M getting the geometrical factor in the form:

$$G_A^{(1)}(\boldsymbol{k}_K)=2e^{2\pi iK(z_A/a)}\sum_{M\geq 0} i^{Mq+(q/2)}J_{Mq+(q/2)}(d)\times\cos\left[(2M+1)(\Phi-\varphi_A)\frac{q}{2}\right].$$

The cosine factor makes significant angular modulation. Even more, it vanishes for

$$\Phi_j=\varphi_A+\pi(2j+1)/q,\quad j=0,\ldots,q-1, \tag{9}$$

which is manifested as the extinction of these layer lines in diffraction patterns for normal incidence along q directions specified by the angles Φ_j.

C. Parities

As for the conformation of the class $\boldsymbol{Y}^{(1)}$, the Bessel functions of each term are multiplied by a phase factor depending on Φ, coordinates of the orbit representative, and counters K and M. Such multipliers, all having unit absolute value, neither amplify nor diminish contribution of particular terms to diffraction intensity. However, in other conformation classes, parities change some parts of these phase factors to cosine functions: σ_h yields cosine dependence on K and z_A, σ_v on M and φ_A, glide plane on K, M, and φ_A, rotoreflectional plane on K, z_A, and M, and U axis on all four parameters. When two parities are present, each contributes by the corresponding factor. In special positions of orbit representatives this effect may lead to disappearing of some layer lines. Cosine dependence on M and φ_A means that Bessel functions in a sum are scaled by different factors. The effect of this is radial modulation of intensity in comparison to the same layer line of the class $\boldsymbol{Y}^{(1)}$ with equal helical axis. It should be noted that the effects introduced by different parities increase the symmetry group of diffraction distribution, such that $\boldsymbol{S}^{(F)}$ is obtained.

These properties will be more neatly analyzed and illustrated in the rest of this section. To clarify the effects of the first family subgroup and parities, we make a comparative study of the orbits generated by the transversals with the same group of generalized translations [one of $\boldsymbol{T}_q^r(f)$, $\boldsymbol{T}(a)$, $\boldsymbol{T}_{2n}^1(a/2)$, and $\boldsymbol{T}'(a/2)$, Figs. 1–5] and different parities; also, the first family subgroup and coordinates of orbit representatives are the same for all the mutually compared orbits.

The plotted region of $\boldsymbol{k}$ in the figures is a square of the length of 4 Å^{-1}, and all radial and z coordinates of orbit

representatives are given in Å. In order to emphasize the general characteristics, the figures present normalized intensity, i.e., absolute square of $G_A^{(F)}(k)$, as the omitted term $f(k)$ (being system dependent and also a rapidly decreasing function) may make described effects harder to observe. At the top of each figure are the normal-incidence patterns, with $\boldsymbol{k}_{\text{in}}$ along y axis (i.e., $\Phi=0$) unless specified otherwise; below are different patterns along the specified layer lines.

1. Chiral conformation classes: $\boldsymbol{T}_q^r(f)\boldsymbol{P}_n$

In accordance with conclusions of Sec. V B, for nontrivial commensurate helical axis, layer lines are spaced by $1/a$ but in all of them except for $K=0, \pm q/n, \pm 2q/n\ldots$ (equatorial and those spaced by multiple of $1/f=qa/n$ from it) K dependent intensity gap appears. Therefore q/n can be determined from the distance of two layer lines with no intensity gap while r is equal to K value of the layer line with minimal nonzero intensity gap. To find n, i.e., to complete determination of $\boldsymbol{Y}^{(1)}$, one can use gap's width of this layer line; also, information about the order of the principle axis of the isogonal group q may be obtained from rotational invariance of any layer line's intensity distribution. Additional U-axis parity in $\boldsymbol{Y}^{(5)}$ infers the dumping factor $\cos[(Mq-Kp)\varphi_A + 2\pi K\frac{z_A}{a}]$, making patterns sensitive to the coordinate z_A of the orbit representative; also, the extinction of intensity along specific Φ directions is not a general rule any more. Two examples of these classes are in Fig. 6. Note the differences of the equatorial layer line patterns caused by special angular position of the representative atom φ_A, for which vanishes the cosine coefficient multiplying the Bessel function of the lowest nonzero order 36 in $G^{(5)}(\boldsymbol{k}_0)$ for $\boldsymbol{T}_{36}^5(1\ \text{Å})\boldsymbol{D}_6$. Also, extinction of layer line $K=\tilde{q}/2=3$ along $q=36$ directions is clearly visible from intensity distribution along these lines for both orbits.

2. Conformation classes $\boldsymbol{T}(a)\boldsymbol{P}_n$

At first, here belong both linear conformation classes $\boldsymbol{Y}^{(14)}=\boldsymbol{T}(a)$ and $\boldsymbol{Y}^{(15)}=\boldsymbol{T}(a)\boldsymbol{C}_{1h}$ (Fig. 5). Their geometrical factors are constant functions along fixed layer line. Still, these two classes are easily distinguished: as for $\boldsymbol{Y}^{(14)}$ the geometrical factor is the same for all the layer lines, while for $\boldsymbol{Y}^{(15)}$, due to the additional horizontal mirror plane σ_h, it depends on K and z_A through the scaling factor $\cos(2\pi K z_A/a)$.

Nonlinear transversals of this type contain the first family subgroup $\boldsymbol{L}^{(1)}=\boldsymbol{T}(a)\boldsymbol{C}_n$: $\boldsymbol{Y}^{(1_1)}$, $\boldsymbol{Y}^{(2)}$, $\boldsymbol{Y}^{(3)}$, $\boldsymbol{Y}^{(6)}$, $\boldsymbol{Y}^{(9)}$, and $\boldsymbol{Y}^{(11)}$ (Fig. 2). As in this case $p=0$, geometrical factor for each K contains the same Bessel functions with their orders being multiple of n. The distinction between classes are additional symmetries, not present in $\boldsymbol{Y}^{(1_1)}$.

For the conformation classes $\boldsymbol{Y}^{(1_1)}$ and $\boldsymbol{Y}^{(3)}$ the diffraction patterns are shown in Fig. 7. The layer lines' patterns are K independent and identical for both orbits since the only difference is K-dependent multiplier of Bessel functions common for all the terms in the sum. However, instead of phase $e^{i2\pi K z_a/a}$ for $\boldsymbol{Y}^{(1_1)}$, due to σ_h this factor is $\cos(2\pi K z_A/a)$ for $\boldsymbol{Y}^{(3)}$. Consequently, intensity of Kth layer line of $\boldsymbol{Y}^{(3)}$ equals to intensity of $\boldsymbol{Y}^{(1_1)}$ dumped by the square of this cosine

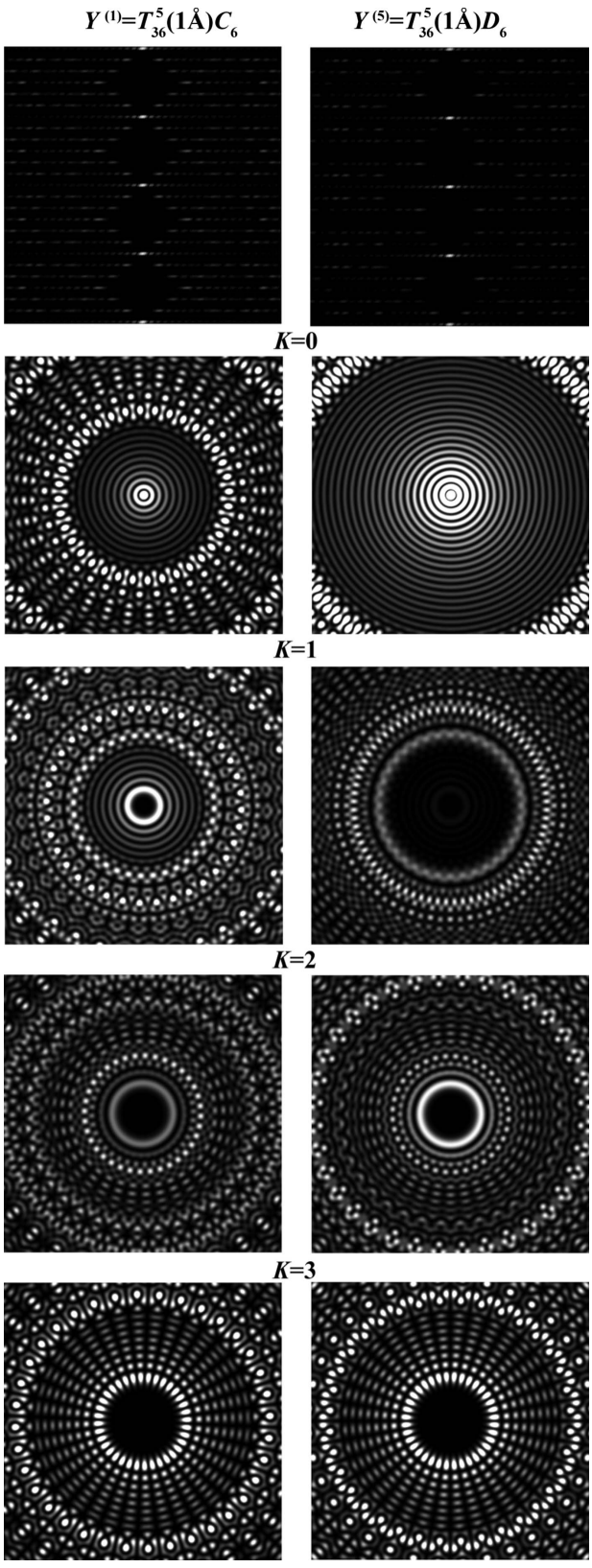

FIG. 6. Simulated diffraction space for orbits $\boldsymbol{Y}^{(1)}=\boldsymbol{T}_{36}^5(1\ \text{Å})\boldsymbol{C}_6$ (left) and $\boldsymbol{Y}^{(5)}=\boldsymbol{T}_{36}^5(1\ \text{Å})\boldsymbol{D}_6$ (right), with orbit representatives at $\boldsymbol{r}_A=(5,5\pi/72,0.45)$. Top: normal incidence patterns. Bottom: density plot of the square of the geometric factor along lines $K=0,\ldots 3$ (these are all different layer lines, as $\tilde{q}=6$).

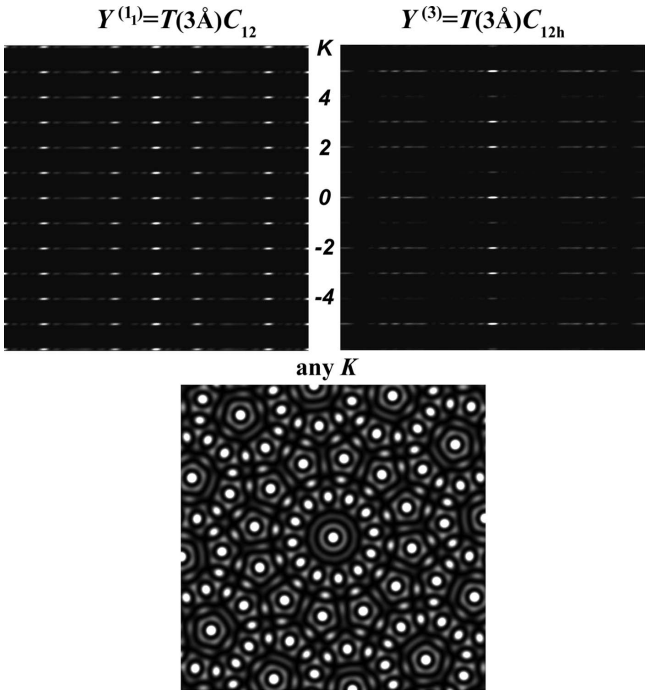

FIG. 7. Simulated diffraction space for orbits $\mathbf{Y}^{(1_1)}=\boldsymbol{T}(3\ \text{Å})\boldsymbol{C}_{12}$ and $\mathbf{Y}^{(3)}=\boldsymbol{T}(3\ \text{Å})\boldsymbol{C}_{12h}$. Bottom: density plot of the square of the geometric factor along arbitrary layer line K. Top: normal incidence patterns; while $|G_A^{(1_1)}(\boldsymbol{k}_K)|^2$ of all layer lines is the same for $\mathbf{Y}^{(1_1)}$ (left), for $\mathbf{Y}^{(3)}$ (right) intensity of Kth layer line is scaled as $|G_A^{(3)}(\boldsymbol{k}_K)|^2=\cos^2(2\pi K z_A/a)|G_A^{(1_1)}(\boldsymbol{k}_K)|^2$.

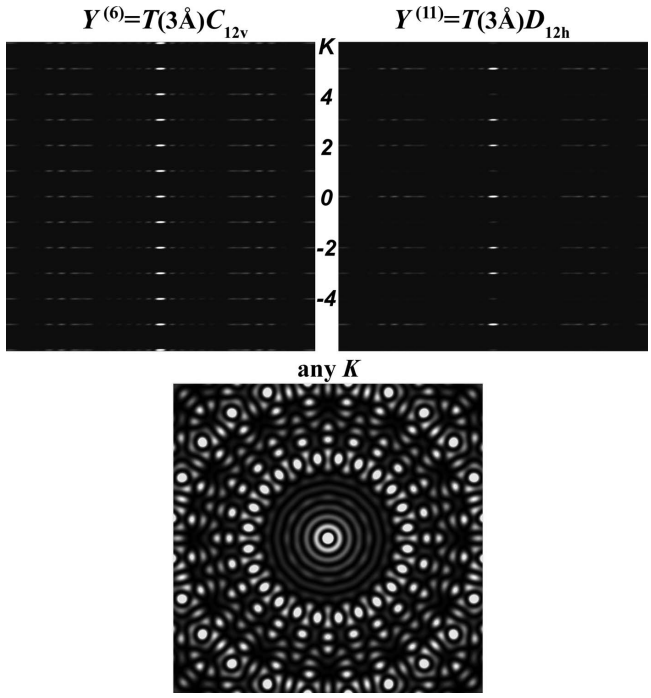

FIG. 8. Simulated diffraction space for orbits $\mathbf{Y}^{(6)}=\boldsymbol{T}(3\ \text{Å})\boldsymbol{C}_{12v}$ and $\mathbf{Y}^{(11)}=\boldsymbol{T}(3\ \text{Å})\boldsymbol{D}_{12h}$. Bottom: density plot of the square of the geometric factor along arbitrary layer line K. Top: normal incidence patterns; while $|G_A^{(6)}(\boldsymbol{k}_K)|^2$ of all layer lines is the same for $\mathbf{Y}^{(6)}$ (left), for $\mathbf{Y}^{(11)}$ (right) intensity of Kth layer line is scaled as $|G_A^{(11)}(\boldsymbol{k}_K)|^2=\cos^2(2\pi K z_A/a)|G_A^{(6)}(\boldsymbol{k}_K)|^2$.

factor. This is observable in the right top diffraction pattern, where some layer lines are almost invisible. As the effect is z_A sensitive, comparison of intensities of distinct layer lines may be used to reveal information on z_A coordinate of the atoms of the conformation class $\mathbf{Y}^{(3)}$.

The additional symmetry σ_v in $\mathbf{Y}^{(6)}$ changes the angular dependence of the Mth term in geometrical factor to $\cos(Mn\varphi_A)$. This results in dumping, and even possible vanishing, of particular terms in $G^{(6)}(\boldsymbol{k}_K)$, which implies that the patterns are not the same as for $\mathbf{Y}^{(1_1)}$ but still mutually identical (as K-dependent phase is common for all the terms). The conformation class $\mathbf{Y}^{(11)}$ has both σ_h and σ_v parities yielding the dumping factor $\cos(2\pi K z_A/a)\cos(Mn\varphi_A)$. Thus, the patterns of the corresponding layer lines are the same as for $\mathbf{Y}^{(6)}$, only their intensities are dumped by $\cos^2(2\pi K z_A/a)$. The diffraction patterns of these two classes are shown in Fig. 8.

The remaining two conformation classes are $\mathbf{Y}^{(2)}$ and $\mathbf{Y}^{(9)}$. Due to rotoreflectional plane in both groups K dependence of the geometrical factors is manifested through multiplier $i^M\cos(2\pi K z_A/a-M\pi/2)$. As it is also M dependent, unlike the previous cases, layer line's pattern is K dependent. Additional vertical mirror plane in $\mathbf{Y}^{(9)}$ as usual introduces $\cos(Mn\varphi_A)$, due to which patterns of $\mathbf{Y}^{(2)}$ and $\mathbf{Y}^{(9)}$ are distinct (Fig. 9). Note that for equatorial line ($K=0$) geometrical factors of both classes contain only even values of M. Value of z_A used in the examples of these two orbits makes some layer lines less intensive than the others. Also, due to very small intensity, differences visible in the intensity distribution along layer $K=1$ layer line lines cannot be noticed at the top diffractions patterns.

3. Conformation classes $T^1_{2n}(a/2)P_n$

The second achiral screw axis characterizes four conformation classes $\mathbf{Y}^{(1_2)}$, $\mathbf{Y}^{(4)}$, $\mathbf{Y}^{(8)}$, and $\mathbf{Y}^{(13)}$ (Fig. 3). Since the first family subgroup is in this case parametrized by $q=2n$ and $r=1$, orders of Bessel functions in the geometrical factors are $(2M-K)n$. In particular, for K even there is the zero-order Bessel function, leading to the bright spot on the Z axis. For odd K, orders of the Bessel functions are odd multiples of n, which results in nonzero intensity gap (equal for all odd lines). Also, as $\tilde{q}=2$ all odd layer lines vanish for Φ_j given by Eq. (9) (for $q=2n$). Therefore, for normal incidence along these directions, patterns look like those formed by systems with pure translational group.

The first class $\mathbf{Y}^{(1_2)}=\boldsymbol{T}^1_{2n}(a/2)\boldsymbol{C}_n$ is a special case of the helical groups discussed above. For them coordinate z_A by no means affects the intensity while extinction angles of odd layer lines is given by Eq. (9), for $q=2n$. Additional symmetries of the other classes introduce different modulating trigonometric factors, which change diffraction patterns (Figs. 10 and 11) although not affecting intensity gaps.

In particular, σ_h results only in the scaling of the intensities by the factor $\cos^2(2\pi K z_A/a)$. This makes some of $\mathbf{Y}^{(4)}$ layer lines hardly visible (compare top panels of Fig. 10) while the patterns of the layer lines (bottom panels) corresponding to the same K are identical for both transversals.

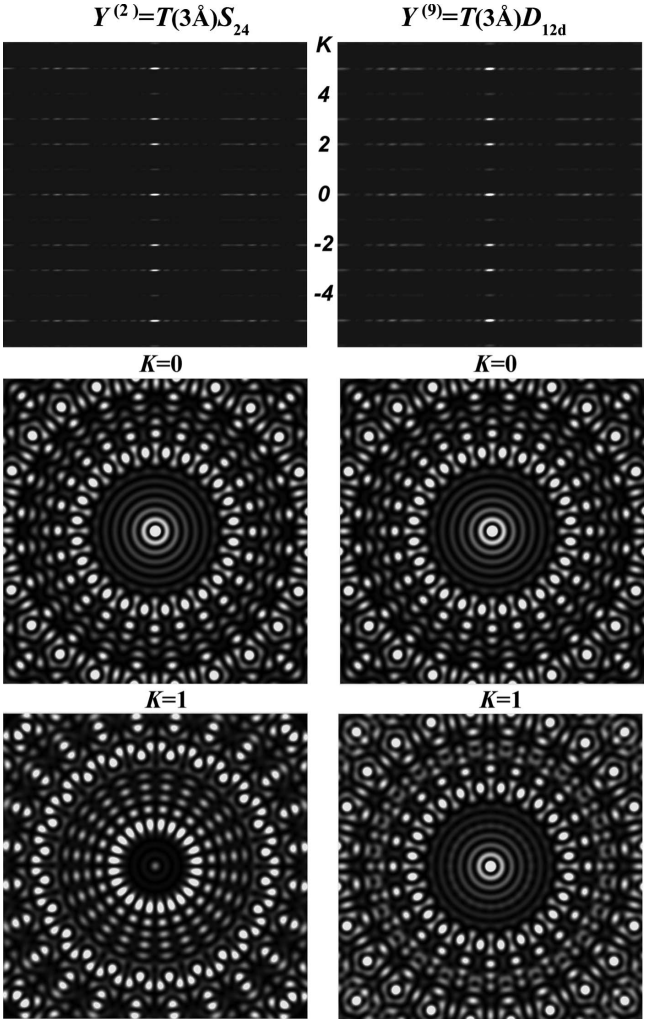

FIG. 9. Simulated diffraction space for orbits $\boldsymbol{Y}^{(2)}=\boldsymbol{T}(3\ \text{Å})\boldsymbol{S}_{24}$ (left) and $\boldsymbol{Y}^{(9)}=\boldsymbol{T}(3\ \text{Å})\boldsymbol{D}_{12\text{d}}$ (right). Top: normal incidence patterns. Bottom: density plot of the square of the geometric factor along arbitrary layer line K.

On the other hand, σ_v changes the intensity distribution along layer lines (compare bottom panels of Figs. 10 and 11). For $\boldsymbol{Y}^{(13)}$, containing both σ_h and σ_v, both effects occur, making Kth layer line pattern the same as for $\boldsymbol{Y}^{(8)}$ but with intensity scaled by $\cos^2(2\pi K z_A/a)$ (Fig. 11). Also, σ_v modifies the directions of extinction of odd layer lines:

$$\Phi_j = \pi(2j+1)/2n, \quad j=0,\ldots,2n-1. \tag{10}$$

4. Conformation classes $T'(a/2)P_n$

In the last three classes $\boldsymbol{Y}^{(7)}=\boldsymbol{T}'(a/2)\boldsymbol{C}_n$, $\boldsymbol{Y}^{(10)}=\boldsymbol{T}'(a/2)\boldsymbol{S}_{2n}$, and $\boldsymbol{Y}^{(12)}=\boldsymbol{T}'(a/2)\boldsymbol{C}_{nh}$ (Fig. 4), group of generalized translations is glide plane $(\sigma_v|a/2)$ while the first family subgroup is $\boldsymbol{L}^{(1)}=\boldsymbol{T}(a)\boldsymbol{C}_n$. Despite this, the term $M=0$ vanishes for K odd due to the factor $\cos(Mn\varphi_A-\frac{K\pi}{2})$ invoked by the glide plane, which makes nonzero intensity gap of these layer lines similar to the case of the transversals with the first family subgroup $\boldsymbol{T}^1_{2n}(a/2)\boldsymbol{C}_n$. For these layer lines the geometrical factor of $\boldsymbol{Y}^{(7)}$ becomes

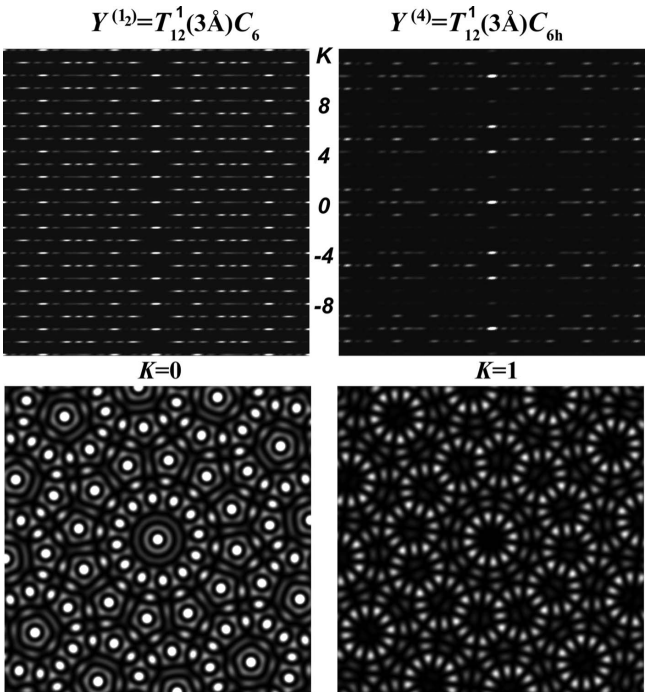

FIG. 10. Top: simulated diffraction patterns for orbits $\boldsymbol{Y}^{(12)}=\boldsymbol{T}^1_{12}(3)\boldsymbol{C}_6$ (left) and $\boldsymbol{Y}^{(4)}=\boldsymbol{T}^1_{12}(3)\boldsymbol{C}_{6h}$ (right) for normal incidence. Below: density plot of the square of geometric factors for $K=0,1$ layer lines (same for both classes). Orbit representatives are at $\boldsymbol{r}_A=(5,5\pi/72,0.45)$. Extinction along 12 directions is clearly visible from density plots of $K=1$ line.

$$G^{(7)}_A(\boldsymbol{k}_K) = 2e^{2\pi i K(z_A/a)} \sum_{M>0} \sin(Mn\varphi_A) i^{Mn} J_{Mn}(d) \sin(Mn\Phi).$$

The last factor, characteristic for all three classes, leads to the extinction of odd layer lines along the $2n$ normal-incidence directions:

$$\Phi_j = \pi j/n, \quad j=0,\ldots,2n-1. \tag{11}$$

This is clearly illustrated on the left $(\Phi=0)$ of Figs. 12–14.

Intensity distribution along the Kth layer line of $\boldsymbol{Y}^{(7)}$ (Fig. 12) is identical to that of $\boldsymbol{Y}^{(12)}$ (Fig. 14) except that the intensity of the latter is dumped by $\cos^2(2\pi K z_A/a)$ (due to this only diffraction patterns for normal incidence are shown in Fig. 14). There are only two different patterns: one for odd K and another for even K layer lines. This does not apply to the remaining class $\boldsymbol{Y}^{(10)}$ as due to rotoreflection symmetry each layer line may be different (Fig. 13).

VI. DISCUSSIONS

Various properties of the diffraction distribution can be used to determine the conformation class. One starts with determination of the group parameters of the first family subgroup $\boldsymbol{L}^{(1)}$. The distance between the gapless layer lines gives value of $1/f$ for both commensurate and incommensurate structures. Several first intensity maxima along these layer lines, corresponding to the first extremes of $J_0(d)$, can be used to determine diameter D_A of the orbit (i.e., radial coordinate $D_A/2$ of the representative atom).

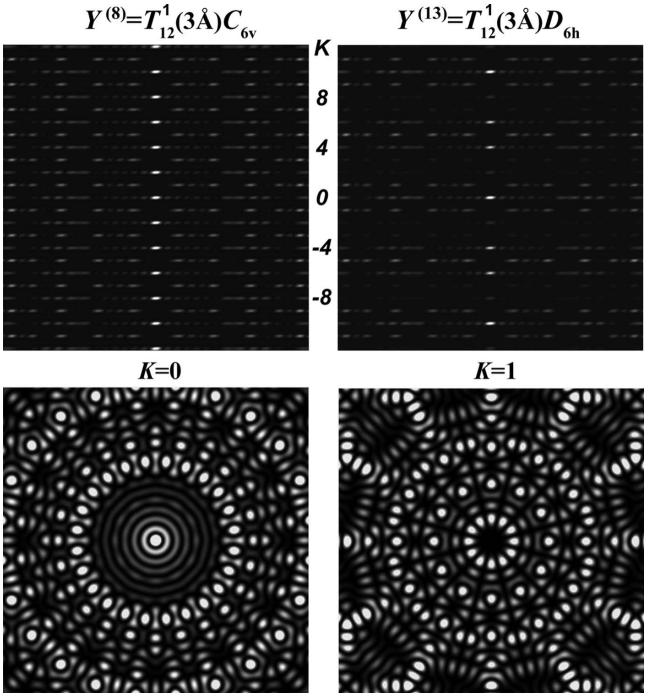

FIG. 11. Top: simulated diffraction patterns for orbits $\boldsymbol{Y}^{(8)}=\boldsymbol{T}^{1}_{12}(3)\boldsymbol{C}_{6v}$ (left) and $\boldsymbol{Y}^{(13)}=\boldsymbol{T}^{1}_{12}(3)\boldsymbol{D}_{6h}$ (right) for normal incidence. Below: density plot of the square of geometric factors for $K=0,1$ layer lines (same for both classes). Orbit representatives are at $\boldsymbol{r}_A=(5,5\pi/72,0.45)$. Extinction along 12 directions is clearly visible from density plots of $K=1$ line.

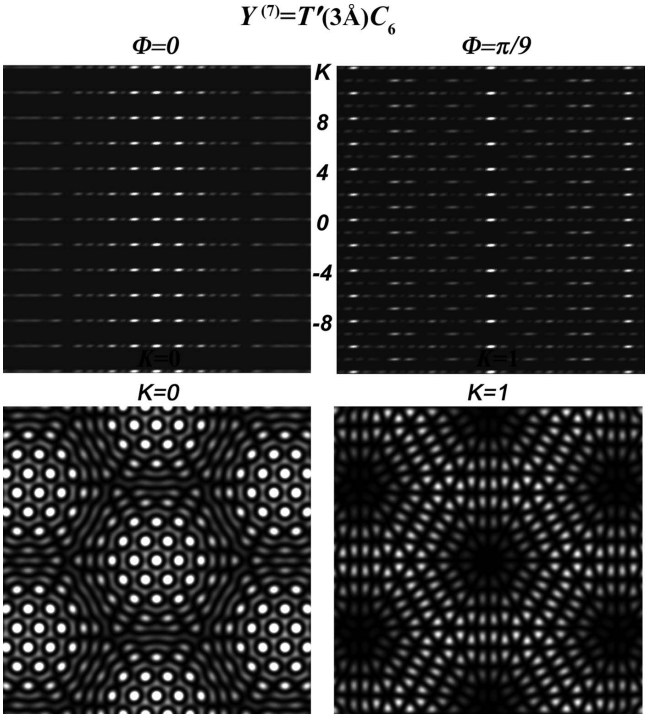

FIG. 12. Diffraction space for $\boldsymbol{Y}^{(7)}=\boldsymbol{T}'(3)\boldsymbol{C}_6$. Top: diffraction patterns for normal incidence for two values of Φ; extinction of odd layer lines is illustrated on left (Φ=0). Bottom: patterns of the layer lines $K=0,1$.

In incommensurate systems, the layer lines are dense. The least gap is for $\tilde{M}=\pm 1$, and positioned at $k_z=\mp n/Qf+\tilde{K}/f$ and $k_\perp=x_{n,1}/\pi D_A$ (or positions of next peaks if necessary), which is sufficient to find Q/n and n, respectively. Then it remains to determine whether the conformation class is $\boldsymbol{Y}^{(1')}$ or $\boldsymbol{Y}^{(5')}$: only if normalized intensity of layer lines is independent of K does the system has no U symmetry. The most prominent fingerprint of incommensurability is full axial symmetry of the distribution along any layer line. Indeed, in commensurate cases sufficiently far from the origin, superposition with higher terms breaks axial symmetry of the distribution. However, real experiments can hardly distinguish between incommensurate and commensurate cases since only limited area around $k_\perp=0$ is visible; within this region layer lines do not seem dense while there is no proof that the axial symmetry of the visible region can be extended out of it. Therefore, together with n and f one finds rational q/r approximating irrational parameter Q.

In commensurate systems the distance between the adjacent layer lines is $1/a=1/\tilde{q}f$, giving $\tilde{q}$; alternatively, $\tilde{q}$ equals the ordinal of the first gapless line above the equatorial one. The next step is to single out the layer line with the narrowest intensity gap: its height (values of the corresponding K) is helicity parameter r; also, the leading term is $J_n(d)$ while the gap radius $x_{n,1}/\pi D_A$ reveals n (and q afterwards). Alternatively, q (and then n) can be found as the order of the principle axis of diffraction space (i.e., of pattern along any layer line).

If $\tilde{q}$ is greater than two, the system is chiral. As in the case of incommensurate systems, it remains to determine if the lines are of the same or varying normalized intensities, which corresponds to the first and fifth conformation classes, respectively. Note only that diffraction does not distinguish between left and right chiral conformations, meaning that the above procedure gives either r or $\tilde{q}-r$ as an irremediable ambiguity.

The achiral classes are mutually distinguished as follows. When all layer lines are gapless, then $\boldsymbol{L}^{(1)}=\boldsymbol{TC}_n$ and $\boldsymbol{Y}^{(F)}$ has no glide plane symmetry. If only even layer lines are gapless, then the first family subgroup is either $\boldsymbol{TC}_n$ with glide plane being additional symmetry or $\boldsymbol{T}^{1}_{2n}\boldsymbol{C}_n$. To distinguish between these two cases it is necessary to analyze the equatorial line: if the circles (their number or radii) can be explained by J_0 and J_{2n}, then $\boldsymbol{L}^{(1)}=\boldsymbol{T}^{1}_{2n}\boldsymbol{C}_n$, while J_0 and J_n accommodate to $\boldsymbol{L}^{(1)}=\boldsymbol{TC}_n$ combined with glide plane. In fact, in the latter case for K even, the number of circles is less while for odd K, the term J_n is present, which results in the more densely filled patterns.

Once $\boldsymbol{L}^{(1)}$ is found, it remains to determine whether the system additionally has some of the parities σ_h, U, σ_v, or $\boldsymbol{S}_{2n}$. The following analysis applies to classes whose $\boldsymbol{L}^{(1)}$ is $\boldsymbol{TC}_n$ without any extra glide plane. First, notice that, if the system has none of these extra symmetries, the normalized intensity of all layer lines is independent of K. Presence of the vertical mirror plane σ_v does not affect this K independence. However, σ_v changes the influence of φ_A in terms with nonzero Bessel functions in the geometrical factor. For n odd there is an evident distinction in Φ dependence of diffraction intensity: the order of the principle axis of diffraction space is halved in presence of σ_v. On the other hand, for

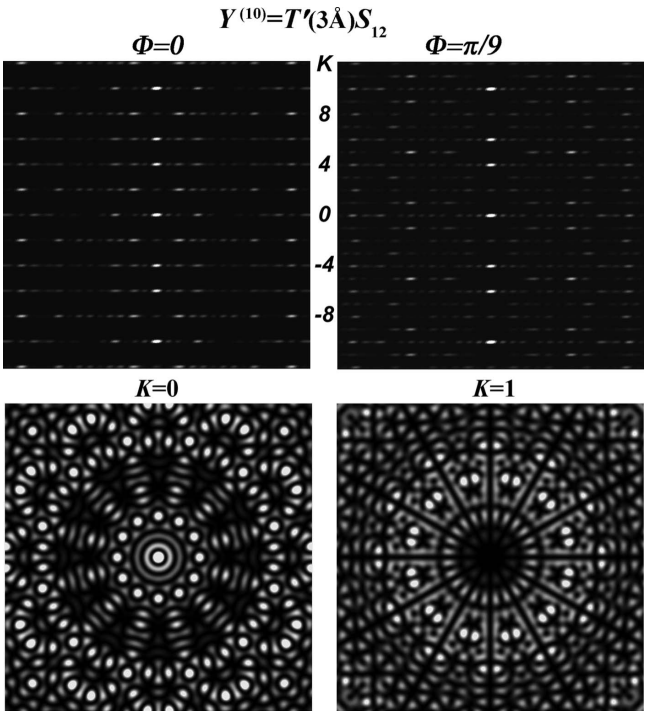

FIG. 13. Diffraction space for $\boldsymbol{Y}^{(10)}=\boldsymbol{T}'(3\ \text{Å})\boldsymbol{S}_{12}$. Top: diffraction patterns for normal incidence for two values of Φ; extinction of odd layer lines is illustrated on left ($\Phi=0$). Bottom: patterns of the layer lines $K=0,1$.

n even $\boldsymbol{S}^{(F)}$ is unaffected by addition σ_v, as it already includes spatial inversion, meaning that it is difficult to differ experimentally between patterns of even n classes with and without vertical mirror plane. Presence of σ_h introduces K dependence of normalized intensity through factor $\cos^2(2\pi K z_a/a)$ but in all layer lines the peak positions remain the same. If, however, peak positions are no longer the same for all layer lines, i.e., they depend on counter K, we have either U or $\boldsymbol{S}_{2n}$ symmetry, which are easily distinguished analyzing equatorial layer line: only $\boldsymbol{S}_{2n}$ causes the terms with M odd to disappear. If several parities are symmetries of the studied class, these effects will combine.

Next we give the algorithm for $\boldsymbol{L}^{(1)}=\boldsymbol{T}^1_{2n}\boldsymbol{C}_n$. If there are no extra parities we have two different types of intensity distribution: one for odd and the other for even layer lines, each of them independent of K. Horizontal mirror plane infers the same changes as explained for $\boldsymbol{TC}_n$. However, the presence of vertical mirror plane can be indicated by odd layer lines for which σ_v affects the manner of φ_A dependence of the leading term in geometrical factor. Note that the symmetry of diffraction space is $\boldsymbol{S}^{(F)}=\boldsymbol{D}_{2nh}$, independently of the presence of any parity. Again, the effects of σ_v and σ_h are combined in $\boldsymbol{Y}^{(13)}$.

It remains to consider $\boldsymbol{L}^{(1)}=\boldsymbol{TC}_n$ combined with glide plane. If there is no more symmetries, the odd layer lines have identical normalized intensities. However, for even K, intensity is K dependent and also the peaks positions are not identical. Previous conclusions for additional σ_h apply to odd layer lines. As for $\boldsymbol{S}_{2n}$, it results in K dependence of normalized intensity for odd layer lines; even the peak positions may not remain the same.

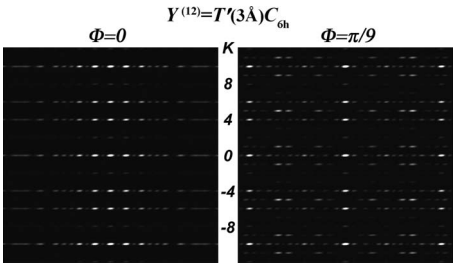

FIG. 14. Diffraction space for $\boldsymbol{Y}^{(12)}=\boldsymbol{T}'(3\ \text{Å})\boldsymbol{C}_{6h}$. Top: diffraction patterns for normal incidence for two values of Φ; extinction of odd layer lines is illustrated on left ($\Phi=0$). Patterns of the layer lines $K=0,1$ are identical to those of $\boldsymbol{Y}^{(7)}$ (Fig. 12).

The geometrical factors (Table II) are straightforwardly applied to the systems composed of several orbits. If a symmetry group of such a system is $\boldsymbol{L}^{(F)}$ ($F=1,\ldots,13$), all the orbits of the system should be enumerated; then each of them is to be found in column 2 of the Fth part of Table I, and the corresponding conformation class is in the first column of the same row. Finally, substituting individual scattering amplitudes of these conformation classes in Eq. (2) gives total scattering amplitude. The symmetry of the distribution is the intersection of the symmetries of the included conformation classes, and at least it is equal to $\boldsymbol{P}^{(F)}_{\mathcal{I}}$, being the isogonal group $\boldsymbol{P}^{(F)}$ of $\boldsymbol{L}^{(F)}$, extended by spatial inversion.

Recently, this symmetry based method has been applied to singe-wall carbon nanotubes.[8] The fact that all such tubes are single-orbit systems (of the type $\boldsymbol{Y}^{(5)}$; see Ref. 9) significantly facilitates the analysis of diffraction patterns. Also, as symmetry uniquely determines the tube structure this means that in theory one can characterize the tube solely from the diffraction patterns analysis. In practice some of symmetry related features may not be visible in the experiment due to the low scattering power of carbon or experimental limitations. Nevertheless, this method definitely adds some information necessary for unique characterization of tubes.

Of course, system whose orbits consist of diverse atoms are the most complicated cases for the analysis of diffraction patterns. Applying the above procedure for calculating diffraction intensity enables fast simulation of the patterns and their further analysis. As an example we consider the case of monolayer MoS_2 armchair nanotube having $\boldsymbol{L}=\boldsymbol{T}^1_{2n}(a/2)\boldsymbol{C}_{nh}$ as its full symmetry group. This system consists of a pair of sulfur planes with a metal plane between them. Each plane can be reconstructed from a single atom so this system contains three orbits in total: all of them are of type $\boldsymbol{Y}^{(1_2)}$ (two orbits with S atoms and one with Mo). Calculated intensities for x-ray diffraction are shown in Fig. 15. Clearly, from shown normal-incidence pattern of tube (10,10), it follows that $\tilde{q}=2$ and $r=1$ while the distance between the layer lines gives translational period $a=3.16$ Å. Oscillation of the intensity along the layer lines is quite dense due to high diameter value and interference effects between individual orbit scattering amplitudes. It turns out that the gap of first layer line is not sufficient for finding n as the first peak is quite broad (this is actuality related to the σ_v symmetry of the tube). Nevertheless, n can be unequally determined by comparison with simulated intensities for the next-neighbor armchair tubes, i.e., tubes (9,9) and (11,11).

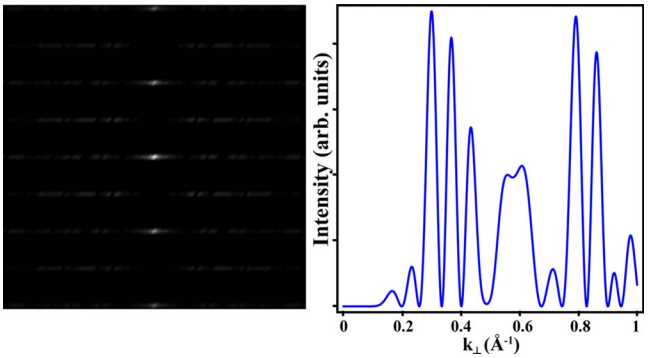

FIG. 15. (Color online) Simulated diffraction intensity for MoS_2 nanotube. Left: normal incidence pattern for tube (10,10); right: intensity along first layer line $K=r=1$.

Finally, let us stress out that the presented results are obtained within kinematical approximation. Still, the symmetry of the diffraction space is model independent. In this context, it should be noted that the range of k is restricted in the real experiment, which leads to considerably fast fading of the patterns with k due to atomic scattering amplitude $f(\boldsymbol{k})$. This may cause that some of the features discussed above are not easily visible. However, this varies with the type of the used beam.

Although many of the symmetry parameters can be determined on the basis of the analysis of the experimentally obtained diffraction patterns (as discussed above), the full symmetry determination is possible only by finding the matching of the measured diffraction pattern with the corresponding one obtained by the numerical simulations. This is due to the complexity of the diffraction images, especially in a case where the system under consideration is built of many conformation classes.

This work is supported by the Serbian Ministry of Science (Project No. ON141017) and EU Contract No. FP6-INCO-WBC-SSA project NanoLabFor.

*tanja37@afrodita.rcub.bg.ac.yu; http://www.nanolab.rs

[1] B. K. Vainshtein, *Fundamentals of Crystals: Symmetry, and Methods of Structural Crystallography* (Springer-Verlag, Berlin, 1994).

[2] B. K. Vainshtein, *Diffraction of X-Rays by Chain Molecules* (Elsevier, New York, 1966).

[3] I. Milošević and M. Damnjanović, Phys. Rev. B **47**, 7805 (1993).

[4] John M. Cowley, *Diffraction Physics* (Elsevier, Amsterdam, 1986).

[5] L. Michel, Rev. Mod. Phys. **52**, 617 (1980).

[6] I. Milošević, R. Živanović, and M. Damnjanović, Polymer **38**, 4445 (1997).

[7] M. Damnjanović, T. Vuković, I. Milošević, and B. Nikolic, Acta Crystallogr., Sect. A: Found. Crystallogr. **57**, 304 (2001).

[8] T. Vuković and M. Damnjanović, Nanotechnology **18**, 375708 (2007).

[9] M. Damnjanović *et al.*, Phys. Rev. B **60**, 2728 (1999).